FLARES FROM THE GIANT AR 9433 ON 24 APRIL 2001

ANITA JOSHI, RAMESH CHANDRA and WAHAB UDDIN
State Observatory, Naini Tal, 263 129, India
(e-mail: anita@upso.ernet.in, ramesh@upso.ernet.in, wahab@upso.ernet.in)

(Received 4 February 2003; accepted 28 June 2003)

Abstract. We present Hα CCD observations of three small-to-medium-size two-ribbon flares observed in the giant AR 9433 on 24 April 2001. Flare observations at other associated wavelengths (e.g., soft X-rays (SXR), hard X-rays (HXR), microwaves (MW)) obtained from archives are also presented and compared. We have tested the Neupert effect for the most energetic third flare. The flare observations are in agreement with the thick-target model. In the case of this flare the HXR emitting electrons appears to be the heating source of SXR and Hα emissions. The flares are also studied in EUV and UV emissions using TRACE data. We discuss the complexity of the magnetic field using SOHO/MDI magnetograms. The flares are observed to occur in both (f/p) polarity regions in highly sheared magnetic field with emerging flux regions and MMFs.

1. Introduction

NOAA AR 9433, a very large sunspot group observed in April 2001, was a recurrence from the previous rotation cycle AR 9393 during 26 March 2001 to 06 April 2001. In fact, it was the largest naked-eye sunspot of the current solar cycle, spanning 260 Mm from end to end and recurring in the next rotation cycle as AR 9461 (17 May 2001–28 May 2001). The sunspot group appeared at N14 E74 on 18 April 2001 and disappeared over the western limb on 02 May 2001. The group showed a spread along the longitudinal direction and covered a maximum area of 1070 millionths of the solar hemisphere.

The group showed $\beta\gamma\delta$ magnetic configuration. It is one of the most complex magnetic field structures and has a higher than average flare productivity tendency. In this active region, on 24 April 2001 we observed three small-to-medium-size (SF, SF/C3.4, and 1N/M2.1) Hα flares. The flares were observed to occur at the location of the sheared/twisted magnetic field. The role of magnetic shear in the flare process was emphasized by several authors (Zirin and Tanaka, 1973; Van Hoven *et al.*, 1980; Hagyard *et al.*, 1982, 1984; Zirin and Liggett, 1987; Hagyard, 1992; Zhang, 1995; Li *et al.*, 1999; Zhang *et al.*, 2001). However, there are also cases of flares without sheared magnetic field (Mathew and Ambastha, 2000) and sheared magnetic field with no flares (Hagyard and Rabin, 1986). In these cases other conditions such as flux emergence or cancellation took place (Vorpahl, 1973; Zirin, 1983; Martin, Livi, and Wang, 1985; Livi *et al.*, 1989; Wang *et al.*, 1991; Wang and Shi, 1993; Debi Prasad, Ambastha, and Ai, 1998; Zhang and Wang,

Solar Physics **217:** 173–186, 2003.

2002). However, counter-examples are also observed where at the locations of emerging flux regions or magnetic cancellation no flares occur.

As the origin of flares is still not well understood, keeping this in mind, we present here the analysis of three flare events observed on 24 April 2001 in AR 9433 at locations N17 E01, N18 E16 and N18 E01 respectively. The details of our Hα observations and multi-wavelength data sources along with data reductions are given in the next section while results derived by us are presented in the remaining part of the paper.

2. Observations and Data Reduction

The Hα and multi-wavelength data used in this study are described in the following subsections.

2.1. Hα DATA

The observations were made at the State Observatory, Naini Tal, using a Bernhard Halle Hα (6563 Å/0.5 Å) filter and a 15 cm $f/15$ Coudé refractor. Image size was enlarged by a factor of two with the help of a Barlow lens. The 512×512 pixels 12-bit frame transfer CCD camera has a square pixel of 15 μm corresponding to a 0.65 arc sec pixel size. The read-out noise for the system is 31 e^- with a gain of 44.1 e^-/ADU. Dark current of the camera is 56 e^- s^{-1}. The camera controller of the system has a variable read-out rate from 0.5 to 2 MHz. The CCD chip (EEV 37) is cooled to -25 °C by a liquid circulatory unit.

On 24 April 2001 observations were taken from 01:25:27 UT to 06:33:04 UT at a cadence of 5 s to 1 min with a exposure of 20 ms. During the observations the sky was partially cloudy and due to this between the observations some data points were missed. At the end of observations the sky was overcast and a flare of M3.1 class from the same active region at the location (N18 E11) of the second flare could not be observed. The total number of frames used in this investigation is about 800. For data calibration several frames of dark and flat field have also been taken. Dark frames of exposure equivalent to our object frames were taken in the dark-mode of the camera. By de-focusing the solar image and taking quiet-region (mostly center of the Sun) flat field exposures were taken. Processing of the images has been done using IRAF software.

2.2. MULTI-WAVELENGTH DATA

The multi-wavelength data, viz., GOES soft X-rays (SXR), *Yohkoh*/hard X-ray telescope (HXT) (Kosugi *et al.*, 1991) hard X-rays (HXR), Nobeyama radioheliograph (Nakajima *et al.*, 1994; Takano *et al.*, 1997) microwaves (MW) and Type III emissions are analyzed in combination with our Hα data. The flares are also

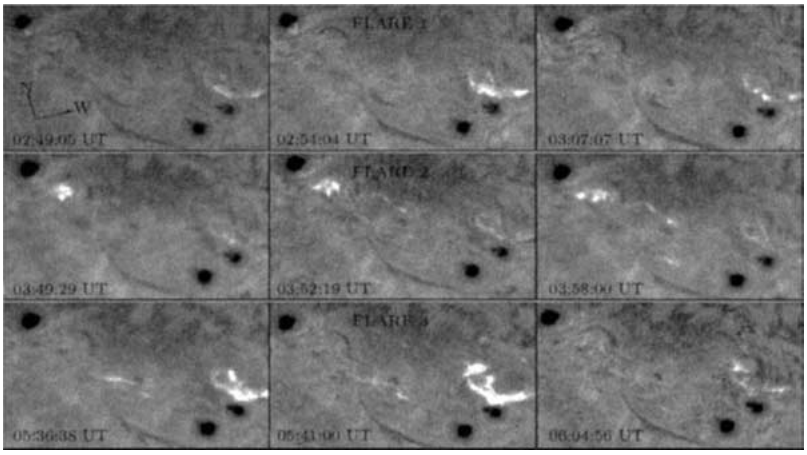

Figure 1. Hα filtergrams (309 arc sec × 199 arc sec) at the start, maxima, and end of the flares.

studied in EUV and UV emissions by using Transition Region and Coronal Explorer (TRACE) data (Handy *et al.*, 1999). TRACE images have a pixel size of 0.5 arc sec within a field of view (FOV) 384 arc sec × 384 arc sec for hot Fe lines (171 Å) and 512 arc sec × 256 arc sec for the UV continuum (1600 Å). Using Solar and Heliospheric Observatory (SOHO)/Michelson Doppler Imager (MDI) (Scherrer *et al.*, 1995) full-disk magnetograms the complexity of the magnetic field is discussed. MDI offers us high temporal resolution (96 min/frame) full-disk data observed on a 1024 × 1024 CCD array with 2 arc sec pixel size. TRACE and MDI images are co-aligned with our Hα images. All aligned images have an 309 arc sec × 199 arc sec FOV. The data were accessed on-line via World Wide Web.

3. Results

3.1. Hα OBSERVATIONS

Figure 1 presents selected Hα filtergrams at the beginning, maxima and ending times of the flares. These are two-ribbon flares. The first and third flares are observed to occur at the same location of the active region and appear to be homologous flares. The time evolution of these flare events structure is best seen in Figure 2. The figure shows iso-intensity plots of the flares in which the isophotes were set at a chosen intensity ratio between flare intensity (I_f) and background intensity (I_b). In the figure, the first isophote was set at a intensity ratio of 1.3 and the increment between the two contour levels was 0.1.

In order to compare our observations with those at other wavelengths in Figure 3 Hα, SXR and MW time profiles are given. In Hα (Figure 3: top) the time profile of the three observed flares is plotted in relative intensity. The relative intensity is the value of peak intensity (I_p) with respect to the background intensity, i.e., I_p/I_b.

TABLE I
Parameters of the flares (F).

F	Hα			SXR			HXR			MW		
	t_F	PF	IMP	t_F	PF	IMP	t_F	PF	IMP	t_F	PF	IMP
1	5.0	1.94	0.39									
2	2.8	1.75	0.63	11	03.49	0.32	0.1	04	40.0			
3	4.4	2.34	0.53	09	21.40	2.38	5.1	88	17.3	4.6	101	22.0

t_F in min.
$PF_{H\alpha}$ and PF_{HXR} in counts, $IMP_{H\alpha}$ and IMP_{HXR} in counts min^{-1}.
PF_{SXR} in 10^{-6} W m^{-2}, IMP_{SXR} in 10^{-6} W m^{-2} min^{-1}.
PF_{MW} in SFU, IMP_{MW} in SFU min^{-1}.

The intensity profile consists of two main parts: an impulsive phase and a gradual declining phase. Its comparison with the SXR (Figure 3: middle) time profile shows remarkable intensity peaks only for the last two flares. The duration of the SXR flare exceeds that of the corresponding Hα emission. It begins about 4 min before the Hα event, attains its peak flux later, and decays several minutes after the Hα flare ceases to be visible. The last two flares are also associated with the HXR. There is only one remarkable peak for microwave (MW) emission (Figure 3: bottom) and that is for the third flare. The nature of the burst is impulsive and it begins 25 s before the Hα event. The third flare emission also occurred at frequencies 200, 245, 410, 500, 610, 1415, 2695, 2800, 4995, 8800, and 15 400 MHz. It is associated with a Type III radio burst of intensity scale 3. This flare is an eruptive event (ERU) and SOHO/LASCO C2 and C3 movies show a CME at about the right time and right span. The CME appeared at 05:54 UT and had a plane-of-sky velocity to the SW of 328 km s^{-1}.

From Figure 3 some basic parameters, viz., rise time t_F and peak flux PF, of the flares are calculated. These two parameters are combined to get the impulsiveness (IMP) of the flare. The IMP = PF/t_F is introduced by Pearson *et al.* (1989). It represents the growth rate of the flare. The values of these parameters are given in Table I. In Hα the growth rate of the second flare is higher than that of the first and third flares. The second flare growth rate is also higher in HXR. In SXR the third flare growth rate is higher.

3.2. The Neupert effect and thermal energy content of the third flare

Figure 4 shows the light curves of third flare emissions at SXR, HXR and Hα wavelengths. As a measure of SXR (maximum at 05:42:27 UT) flux, we used GOES 1–8 Å channel 1 data with 3 s time resolution, while for HXR flux, we used *Yohkoh*, HXT M2 channel data covering the energy range of 32.7–52.7 keV. To check the 'Neupert effect' (Neupert, 1968; Dennis and Zarro, 1993), the time

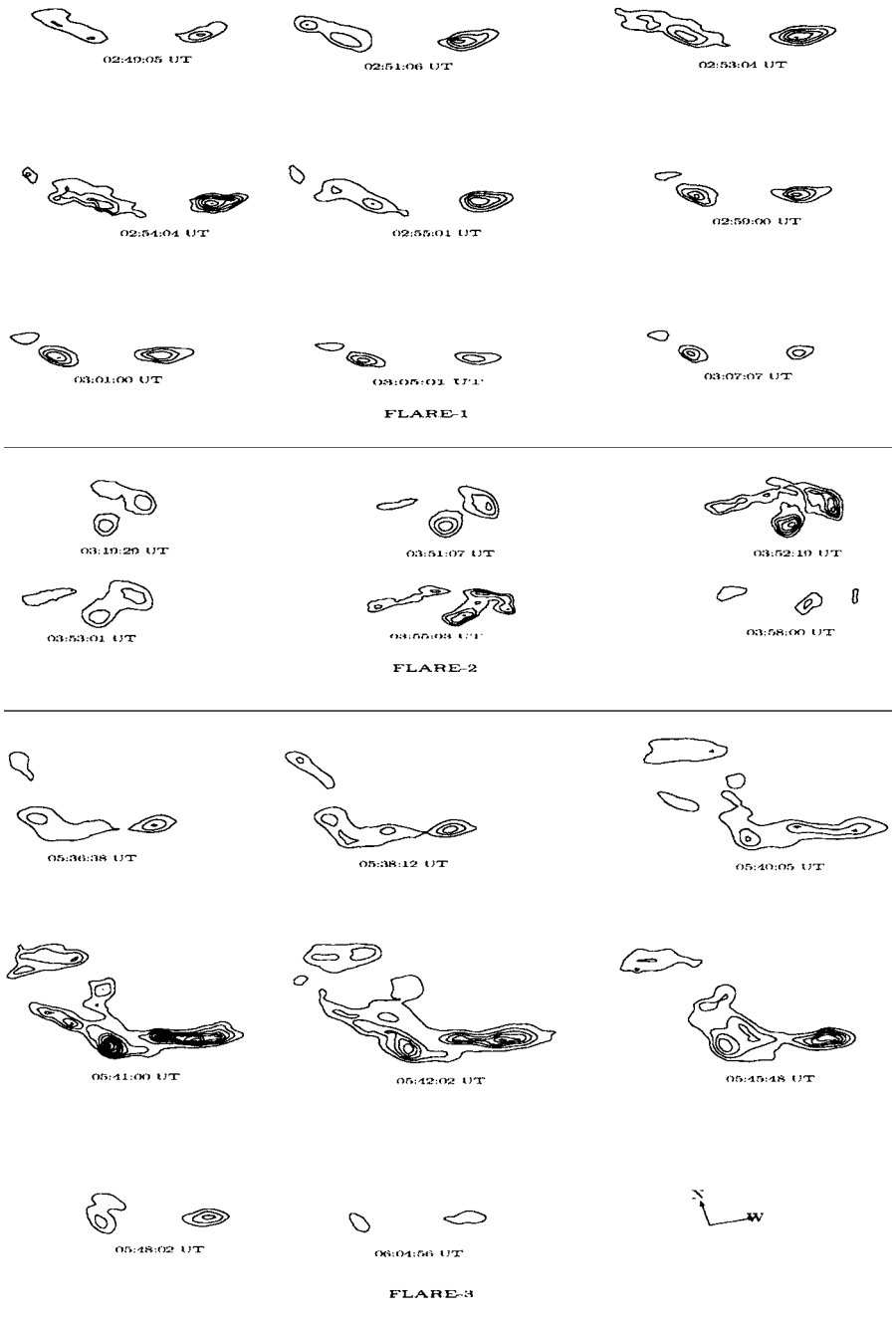

Figure 2. Iso-intensity plots of the flares. The contour levels are 1.3–1.9, 1.3–1.7, and 1.3–2.3, respectively for flare 1, 2, and 3 with an increment of 0.1.

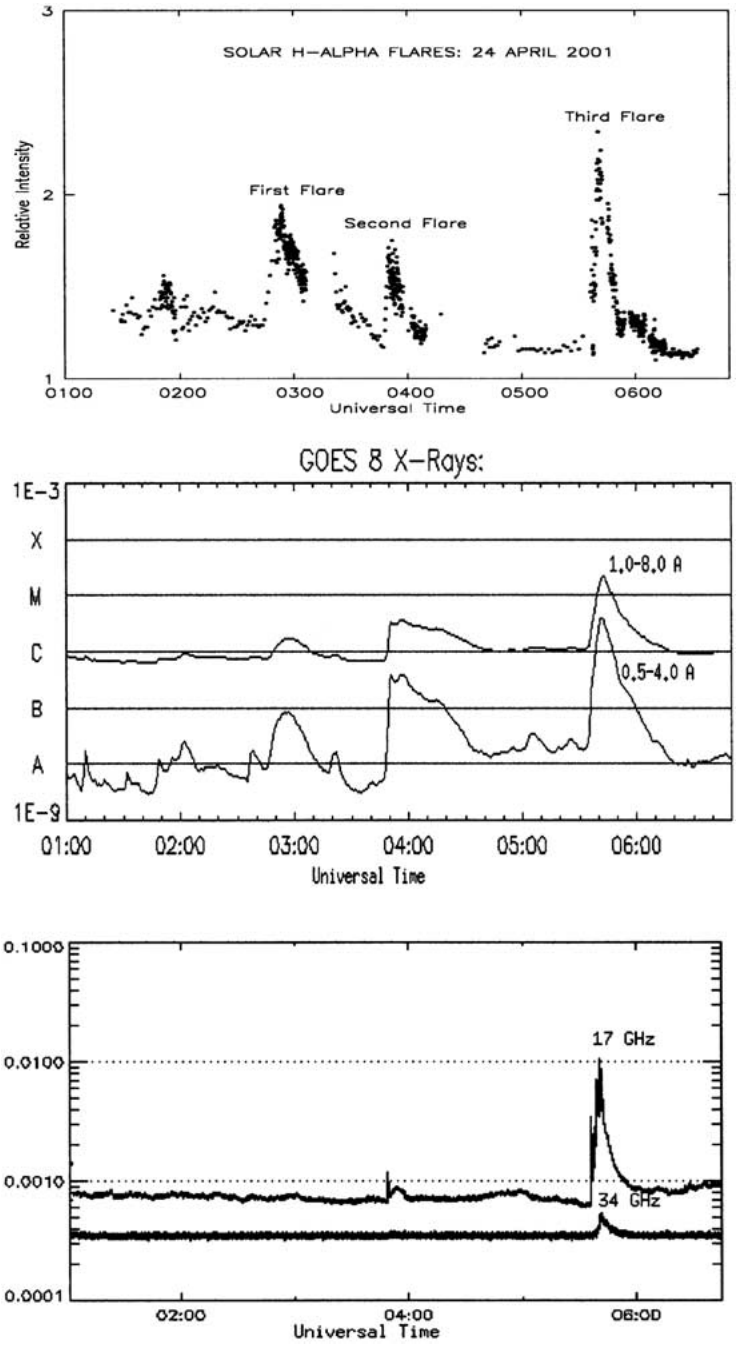

Figure 3. Hα (*top*), SXR (*middle*), and MW (*bottom*) time profiles of the flares.

derivative of SXR emission is also plotted in the figure. The SXR time derivative plot has been computed by taking the average value of the SXR flux over four 3 s intervals and dividing the first difference by 12 s. (Note that this technique is adopted for reducing scatter.) In general we find that the flare shows good correlation between the SXR time derivative and HXR light curve. The derivative peaks after 8 s of HXR emission and drops to zero when the HXR (ended at 05:42:50 UT) drops to background level. At least four and possibly six peaks can be identified in both plots with the peak time agreeing to better than $\pm$ 10 s; the rise and decay times are also very similar. In the figure the derivative peaks before 12 s of Hα emission. The temporal correlation between the Neupert peak and Hα (maximum at 05:41:00 UT) emission suggests that the acceleration of non-thermal electrons was involved in the heating of lower chromosphere.

The thermal energy contained in the SXR-emitting plasma for the third flare may be estimated by

$$E = 3kTn_eV,$$

where k is the Boltzmann constant, T is the plasma temperature, n_e and V are the flare loop density and the emitting volume, respectively. Based on the values of the GOES emission measure EM and volume V an estimate of the flare loop density n_e was obtained as

$$n_e = \sqrt{\frac{EM}{V}}.$$

Following Thomas, Starr, and Crannell (1985) the plasma parameters T and EM were determined from GOES two-channel diagnostics using SSWIDL software. The computed value of T and EM of the hot SXR plasma are 14.33 MK and 2.32×10^{49} cm^{-3}. In a next step we estimate the volume of the SXR-emitting plasma during the flare, for which the length and width of the SXR loop can be estimated from SXT and TRACE images, and the thickness of the loop is taken the same as the loop width. This yields volume V as 18.03×10^{27} cm^3. The electron density of the loop was about 3.59×10^{10} cm^{-3}. The thermal energy contained in the SXR plasma for the third flare is found to be 3.84×10^{30} erg.

3.3. EUV AND UV EMISSIONS

TRACE images in UV (1600 Å) show almost similar morphological evolutions of the flares as in Hα. But as we go to higher temperature (EUV) the similarity is much less. The brightest feature in EUV (171 Å) images is two or more low-lying, slightly inclined and interacting EUV loops. In Figures 5–7 these images of the flares with Hα filtergrams and MDI magnetograms are shown. Times indicated in the images are almost equivalent to those in the optical images and images are for the same FOV (309 arc sec $\times$ 199 arc sec). The first and third flares occurred at the same location with bright flare ribbons and bright flare loops whereas the

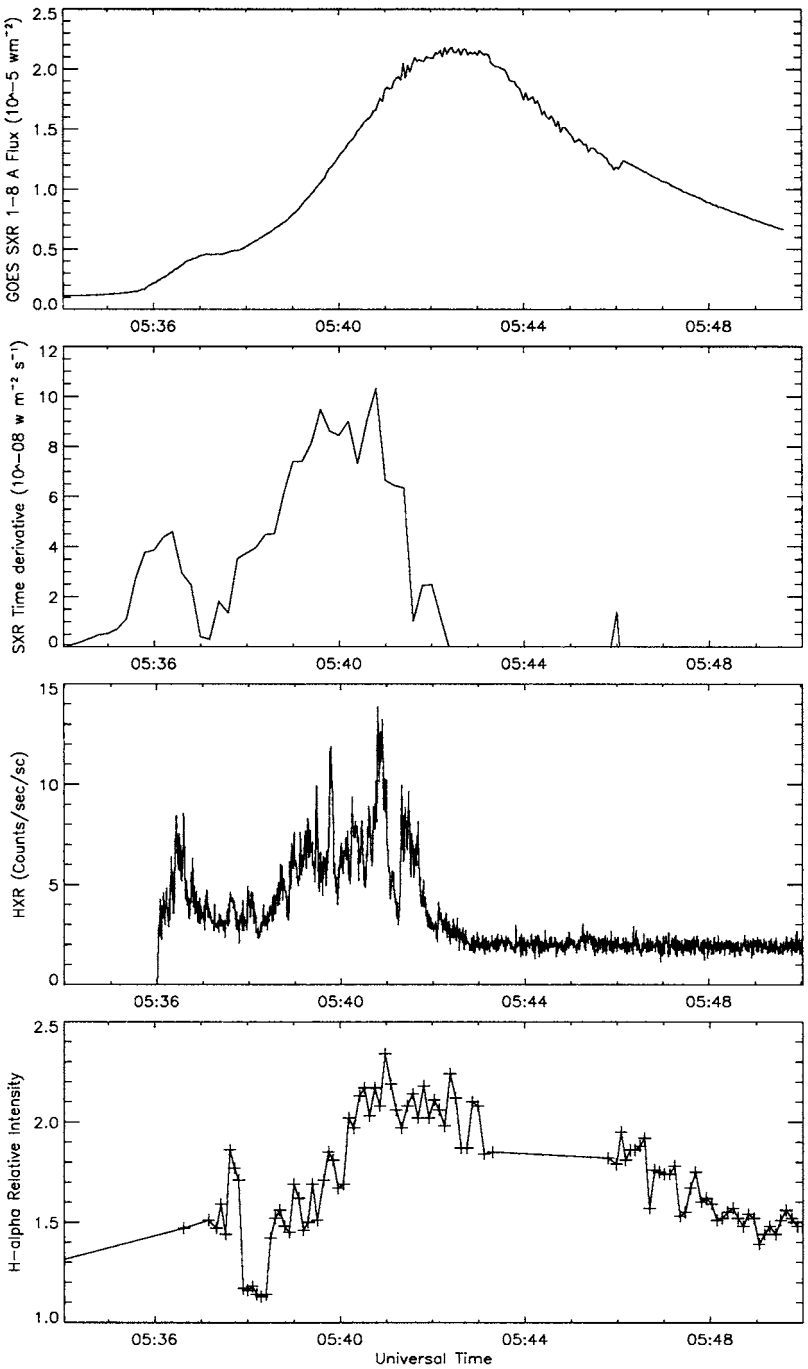

Figure 4. From top to bottom: SXR, time derivative of the SXR, HXR (32.7–52.7 keV) and Hα time profiles of the third flare.

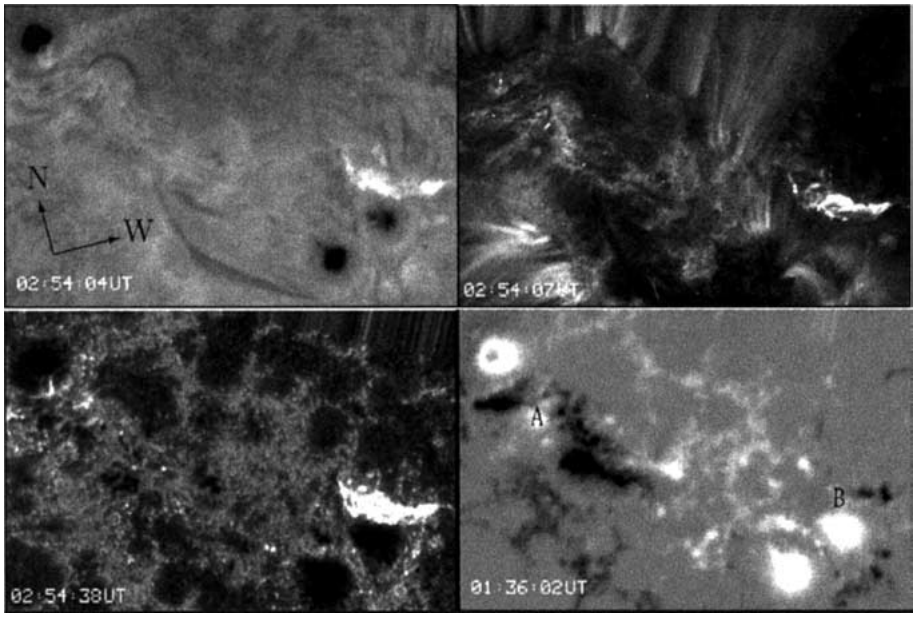

Figure 5. From left to right: Hα, TRACE 171 Å (Fe IX/X ≈ 1 MK), TRACE 1600 Å (UV continuum/C I/Fe II ≈ 0.01 MK) and MDI magnetogram of the first flare.

second flare had low lying coronal loops which faded out slowly. Formation of bright loops joining the flare ribbons occurred presumably due to magnetic reconnection and their disruption was continued during the flares which started eruption of the third flare (SOHO/EIT – *http://lasco-www.nrl.navy.mil/daily_mpg/2001_04/010424_dit_195.mpg* difference movie also shows that the third flare was an eruptive event). The images show flaring in an extended area of the active region and showing the appearance of new EUV loops towards the end of flare. During the second flare at the location of the first and third flares there remains a flare-like brightening, which might be considered as a precursor phase of the most energetic, eruptive third flare.

3.4. Complexity of the Magnetic Field

SOHO/MDI magnetograms presented in Figures 5–7 show complexity of the active region. The elongated sunspot group has three main sunspots of positive (north *n*/preceding *p*) polarity and the active region has negative (south *s*/following *f*) as well as positive polarity at the locations of the flares. The active region was in a $\beta\gamma\delta$-configuration with a magnetic field of medium intensity, but high stress and shear/twist along the polarity inversion line. The Marshall Space Flight Center (*http://magaxpl.msfc.nasa.gov/cgi-bin/gif-walk*) shear map of 23 April 2001 also shows 80°–90° shear at the locations of the flares. For a quantitative measurement of shear along the polarity inversion line on 24 April 2001 we have measured the

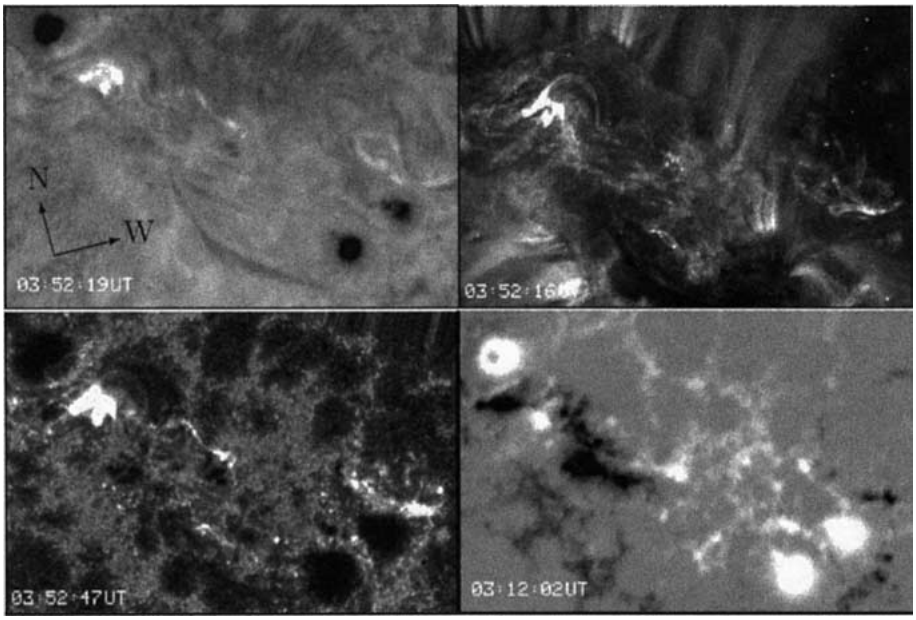

Figure 6. From left to right: Hα, TRACE 171 Å (Fe IX/X ≈ 1 MK), TRACE 1600 Å (UV Cont./C I/Fe II ≈ 0.01 MK) and MDI magnetogram of the second flare.

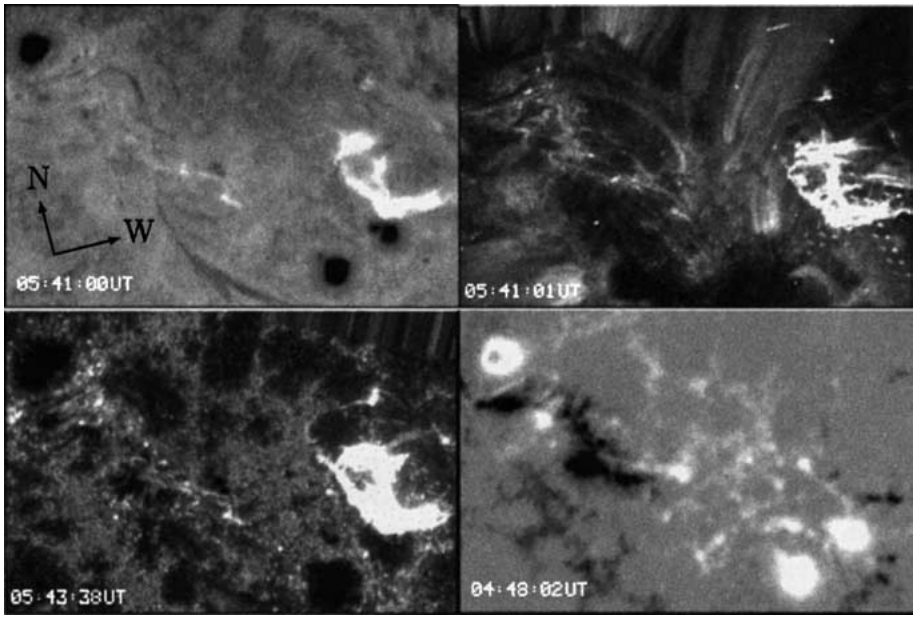

Figure 7. From left to right: Hα, TRACE 171 Å (Fe IX/X ≈ 1 MK), TRACE 1600 Å (UV Cont./C I/Fe II ≈ 0.01 MK) and MDI magnetogram of the third flare.

twisting index (TI) of magnetic neutral line at the flare locations, marked as A and B in Figure 5. The TI of the magnetic neutral line was obtained from the following expression given by Uddin, Pande, and Shelke (1986):

$$TI = \frac{N}{L} + C + \sqrt{\sum (C - C_i)^2},$$

where N represents the number of deviation peaks, L the overall length of the neutral line, C the overall curvature of the neutral line irrespective of the direction of neutral line and $\sqrt{\sum (C - C_i)^2}$ is the sum of i deviations from the mean curvature of neutral line. We find that at location A (7.84) TI is higher than that at location B (1.53). The higher value of TI at location A may be the cause of the large number of flare occurrence at that particular location. The observed flares at location A and B are 10 and 5, respectively.

A detailed examination of the time-sequence magnetograms shows that flux is emerging in the active region at the locations of the flares. To show this, using SOHO/MDI magnetograms, we have calculated the net positive, negative as well as the total flux during 23–24 April 2001 within rectangular areas enclosing the flaring sites A and B. The rectangular area has a box of size 208 arc sec $\times$ 184 arc sec and A (or B) written at the center of the box. The values are plotted in Figure 8. The figure shows increase in positive, negative and total flux values, indicating a flux emergence at these two locations concurring with the flares. The rate of positive, negative, and total flux emergence in flaring site A is 2.45×10^{19}, 4.65×10^{19}, and 7.10×10^{19} Mx h^{-1}, respectively. Similarly, in flaring site B the rate of positive, negative, and total flux emergence is 12.45×10^{19}, 4.68×10^{19}, and 17.13×10^{19} Mx h^{-1}, respectively.

To understand the complexity of the magnetic field here we have also studied a movie of the MDI maps. The movie between 20–26 April 2001 shows counter-streaming of opposite polarity flux concentrations at the two flare sites. An interaction between flux emergence and moving magnetic features, a sign of sunspot decay, which are streaming out from the big positive spots, is also visible. The three major bipoles of the active region emerged close in space and time. It is an activity complex in which smaller-scale flux loops are emerging. New flux interacts with the pre-existing magnetic field, producing recurrent flaring sites, which include the two sites presented in the paper. In these two sites the magnetic field was unstable and reconfigured repeatedly.

4. Discussion and Conclusion

We present and discuss three small-to-medium-size (SF, SF/C3.4, 1N/M2.1) two-ribbon flares observed in the giant AR 9433 sunspot group on 24 April 2001. In these flares, the first and third flares are observed to occur at the same location of the active region and to look like homologous flares. A comparison of the Hα time

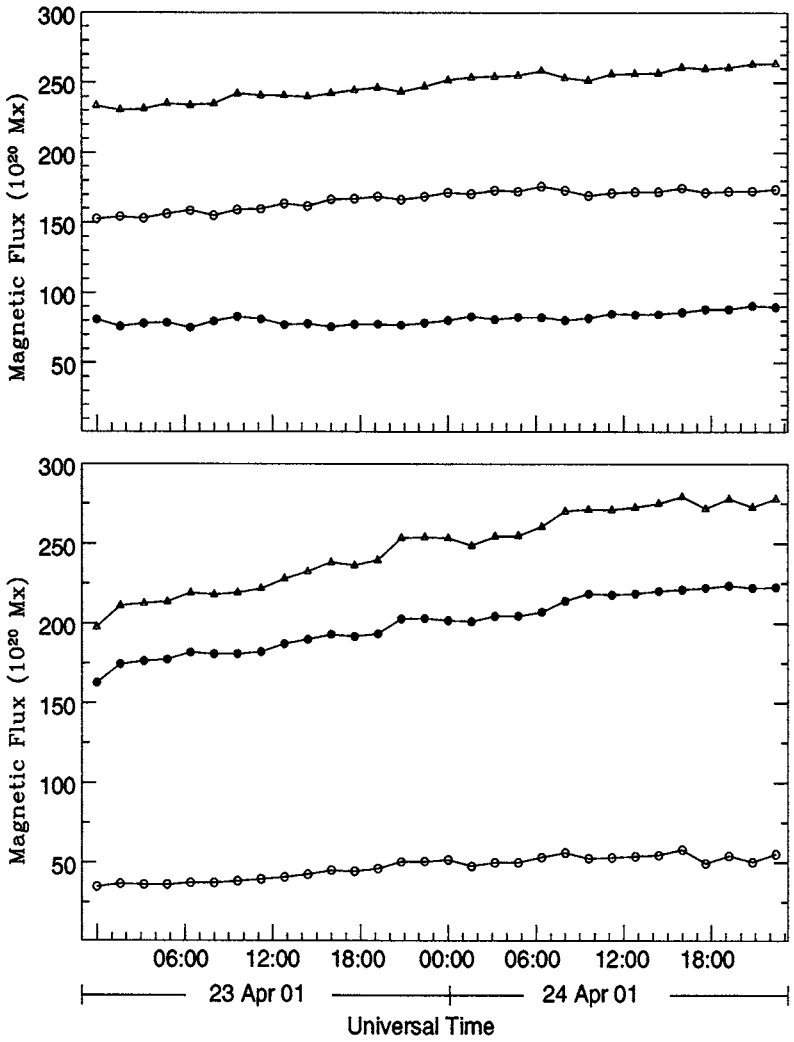

Figure 8. The net positive, negative and total flux during 23–24 April 2001 within 208 arc sec × 184 arc sec rectangular areas enclosing the flaring sites A (*upper panel*) and B (*lower panel*), as marked in Figure 5. The positive, negative and total flux are represented by the *filled circle*, *open circle* and *triangle*, respectively.

profile with the SXR time profile shows remarkable intensity peaks only for the last two (HXR associated) flares whereas in case of the MW time profile there is only one remarkable intensity peak and that is for the third flare. In Hα, SXR, HXR and MW the growth rate of the flares is also calculated and compared.

The third flare is an eruptive event produced emission at almost all wavelengths and associated with a CME. We have tested the Neupert effect for the third flare. This provides a simple, but effective way comparing the timing of the HXR emission and the heating of the plasma. The flare supports the thick-target model

(Brown, 1971) in which the HXR are electron–ion bremsstrahlung produced by non-thermal electrons. The loss of non-thermal electrons energy in the lower corona and upper chromosphere, results in increased SXR (thermal bremsstrahlung) emission. Keeping in mind that the heating of the chromosphere is a complicated process, we also correlated the Hα light curve with the SXR, its derivative and HXR light curves. This implies that the HXR emitting electron is the heating source of SXR and Hα emitting plasma. The coincidence of the relative timings of the peak Hα and SXR flux and the end of HXR emission shows that the flare also supports the electron-beam-driven chromospheric evaporation model. The flare started in the high stratum of the solar atmosphere and goes down from the corona to the chromosphere. In case of this flare it also seems that with time the electrons penetrated to deeper layers and emission started in higher and higher frequencies.

The solar transition region connecting the cool chromosphere and hot corona was studied through the observations of UV and EUV emissions. In these flares TRACE images in UV show almost similar structural details of the flares as in Hα, whereas in EUV collisions and disruptions of low-lying coronal loops are most prominent. It is clear from EUV, UV and Hα images that lower temperature emission sources were well co-aligned at the footpoints of these EUV loops.

The flares are observed to occur in both (f/p) polarity regions at the location of the sheared magnetic field. The role of magnetic shear in the flare process was emphasized by several authors (Zirin and Tanaka, 1973; Zirin and Liggett, 1987; Zhang *et al.*, 2001). Both big and small flares have been reported to occur in the sheared magnetic field at locations A and B. On 24 April 2001 the number of reported flares at location A is larger than that at location B. This may be due to high shear ($TI = 7.84$) of magnetic neutral line at location A. This is in good agreement with the results reported by Uddin, Pande, and Shelke (1986) and Joshi (1995). They reported that the number of flare events increases with the increasing twisting index of the magnetic neutral line.

In the active region at the locations of the flares flux is emerging and existing magnetic features are moving. The first and third flares occurred at the same location towards the leading edge of the p-spot. At that particular location due to new flux interaction with the existing flux (i.e., moving magnetic features) the magnetic field was very complicated, unstable and reconfigured again and again leading to originate recurrent flare activity. Recently, Zhang and Wang (2002) suggested that the repeated flares–CME activities are triggered by the continuous emergence of moving magnetic features.

Acknowledgements

We wish to thank Prof. R. Sagar for helpful comments and suggestions. We also thank Dr L. van Driel-Gesztelyi of Observatoire de Paris for valuable suggestions as well as for providing movie of MDI maps. Thanks to Dr R. Viereck, NOAA Space Environment Center for providing us with 3-s time resolution SXR data.

Special thanks to anonymous referee for constructive comments and suggestions which improved the scientific content of the paper.

References

Brown, J. C.: 1971, *Solar Phys.* **18**, 489.
Debi Prasad, C., Ambastha, A., and Ai, G.: 1998, *Solar Phys.* **179**, 133.
Dennis, B. R. and Zarro, D. M.: 1993, *Solar Phys.* **146**, 177.
Hagyard, M. J.: 1992, *Mem. Soc. Astron. Ital.* **61**, 337.
Hagyard, M. J. and Rabin, D. M.: 1986, *Adv. Space Res.* **6**, 7.
Hagyard, M. J., Cumings, N. P., West, E. A., and Smith, J. E.: 1982, *Solar Phys.* **80**, 33.
Hagyard, M. J., Smith, J. B., Jr, Teuber, D., and West, E. A.: 1984, *Solar Phys.* **91**, 115.
Handy, B. N. *et al.*: 1999, *Solar Phys.* **187**, 229.
Joshi, A.: 1995, *Solar Phys.* **157**, 315.
Kosugi, T. *et al.*: 1991, *Solar Phys.* **136**, 70.
Li, W. *et al.*: 1999, in A. Wilson (ed.), *ESA SP Ser.* **448**, 169.
Livi, S. H. B., Martin, S. F., Wang, H., and Ai, G.: 1989, *Solar Phys.* **121**, 197.
Martin, S. F., Livi, S. H. B., and Wang, J.: 1985, *Australian J. Phys*. **38**, 929.
Mathew, S. K. and Ambastha, A.: 2000, *Solar Phys.* **197**, 75.
Nakajima, H. *et al.*: 1994, *Proc. of the IEEE,* 82, 705.
Neupert, W. N.: 1968, *Astrophys. J.* **153**, L59.
Pearson, D. H., Nelson, R., Kojoian, G., and Seal, J.: 1989, *Astrophys. J.* **336**, 1050.
Scherrer, P. H. *et al.*: 1995, *Solar Phys.* **162**, 129.
Takano, *et al.*: 1997, *Coronal Physics from Radio and Space Observations, (Lecture Notes in Physics)*, Springer-Verlag, Berlin, p. 183.
Thomas, R. J., Starr, R., and Crannell, C. J.: 1985, *Solar Phys.* **95**, 323.
Uddin, W., Pande, M. C., and Shelke, R. N.: 1986, *Bull. Astron. Soc. India* **14**, 91.
Van Hoven, G. *et al.*: 1980, in P. A. Sturrock (ed.), *The Preflare State in Solar Flares*, Colorado Associated University Press, Boulder, p. 17.
Vorpahl, J.: 1973, *Solar Phys.* **28**, 115.
Wang, H., Tang, F., Zirin, H., and Ai, G.: 1991, *Astrophys. J.* **380**, 282.
Wang, J. and Shi, Z.: 1993, *Solar Phys.* **143**, 119.
Zhang, H.: 1995, *Astron. Astrophys.* **297**, 869.
Zhang, J. and Wang, J.: 2002, *Astrophys. J.* **566**, L120.
Zhang, J., Wang, J., Deng, Y., and Wu, D.: 2001, *Astrophys. J.* **548**, L99.
Zirin, H.: 1983, *Astrophys. J.* **274**, 900.
Zirin, H. and Liggett, M. A.: 1987, *Solar Phys.* **113**, 267.
Zirin, H. and Tanaka, K.: 1973, *Solar Phys.* **32**, 173.